

RESIDUAL ATTENTION-ENHANCED MULTI-SCALE DEEP LEARNING FRAMEWORK FOR ROBUST AND CONTINUITY-AWARE LUNG TUMOR SEGMENTATION FROM CT IMAGES

PALYAM MUTHYALA MADHURI¹, DR. VIJAY KUMAR DAMERA²

¹Research Scholar, Koneru Lakshmaiah Education Foundation, Department of Computer Science and Engineering, Hyderabad-500075, Telangana, India

²Assistant Professor, Koneru Lakshmaiah Education Foundation, Department of Computer Science and Engineering, Hyderabad-500075, Telangana, India

E-mail: 'palyammadhuriklu@gmail.com

ABSTRACT

The accurate segmentation of lung tumors in computed tomography (CT) scans is a critical step in computer-aided diagnosis and clinical planning. However, many existing segmentation pipelines remain sensitive to scale variability, boundary ambiguity, and inter-slice inconsistency, which can lead to fragmented masks and elevated false positives in challenging CT cases. However, complex anatomical variations, irregular lesion boundaries, and low tissue contrast often limit the performance of conventional deep learning models. This study introduces a Residual Attention-Enhanced Multi-Scale Deep Learning Framework (RAEMD-Net) designed to achieve robust and precise segmentation of lung tumors from CT images. The framework integrates multi-scale convolutional feature extraction, DenseNet-based residual connectivity, and a bidirectional LSTM module to capture both spatial and contextual dependencies within 3D image sequences. An adaptive attention mechanism dynamically adjusts the feature weights to enhance tumor boundary localization, while a hybrid loss function combining Dice and focal components improves gradient stability and class balance. Extensive experiments conducted on the LUNA16 and NSCLC-Radiomics datasets demonstrate that RAEMD-Net achieves a mean Dice coefficient of 0.96, Jaccard index of 0.94, and Hausdorff distance reduction of 12%, outperforming U-Net, SegNet, and Transformer-based baselines. Ablation analyses further indicate that residual attention contributes most strongly to false-positive suppression, while multi-scale fusion supports edge continuity across heterogeneous tumor sizes. The proposed model achieves computational efficiency through dynamic learning rate scheduling and parameter optimization, making it suitable for real-time deployment in medical imaging systems.

Keywords: *Deep Learning; Multi-Scale CNN; Residual Attention; LSTM Networks; Lung Tumor Segmentation; CT Imaging; Computer Vision; Hybrid Loss Optimization; Scientific Computing*

1. INTRODUCTION

Lung cancer remains one of the leading causes of cancer deaths worldwide and holds a significant proportion of the world's cancer-related mortality. Accurate and early detection is paramount because patient outcome is greatly influenced by early diagnosis and proper treatment planning. For this reason, automatic lung nodule segmentation from CT scans is a critical foundation for clinical decision-making. Although manual drawing by radiologists remains standard practice, it is labour-intensive, time-consuming, and very prone to inter- and intra-observer variation. Such drawbacks are

most noticeable in small, irregularly contoured, or structurally sophisticated nodules, which in routine examinations are often missed. Such challenge has necessitated the emergence of automated segmentation systems, with deep learning as a viable solution owing to its ability to achieve high accuracy and efficiency in identifying intricate patterns [1-2].

Though there have been significant improvements, recent deep learning techniques used in lung nodule segmentation continue to face inherent challenges. The majority of traditional architecture is either dedicated to fine local details or to large contextual features but rarely addresses both. As a result, minor or small nodules are often missed, and false positives remain an issue. Heterogeneity of

nodules—ranging from very tiny to big, irregular, or juxta-pleural sizes—contributes to the challenge of segmentation. Another problem is created by the three-dimensional CT scanning in which nodules appear on numerous slices. Classical models that process slices in isolation are prone to ignore inter-slice dependencies and therefore end up with incomplete or fragmented segmentation. Besides, deep learning models tend to have slow convergence, local minima trap, and unsteady training optimization, which further limit their clinical usability [3].

Several representative studies have improved CT nodule delineation through encoder–decoder designs, attention-guided feature refinement, and 3D context modelling; however, many still exhibit performance degradations under low-contrast boundaries, scale variation, and cross-slice discontinuities, motivating a unified solution that jointly addresses these factors.

To address these challenges, this study proposes a novel deep learning framework to capture the local and global contextual information through multi-scale feature fusion. The framework employs residual attention modules, which combine spatial and channel-wise attention with residual connections to direct attention to clinically informative features and eliminate false positives. Moreover, LSTM units are employed in order to capture sequential relationships among CT slices to enhance the continuity and precision of nodule boundaries in three dimensions. In stabilizing and accelerating training, a dynamic learning rate scheduler is utilized so as to enable adaptive optimization and improve convergence.

Accordingly, the need of this study is to develop a clinically reliable segmentation approach that maintains boundary precision across heterogeneous nodule sizes while preserving cross-slice continuity and reducing false positives under realistic CT variability.

Briefly, the model uses multi-scale CNNs, LSTM-based recurrent layers, and residual attention blocks to provide an efficient and computationally strong lung nodule segmentation architecture. By tackling inter-slice dependency, nodule heterogeneity, and optimization stability simultaneously, the architecture is well-positioned to overcome current approaches and move towards more reliable computer-aided diagnosis systems for lung cancer therapy. **The overall workflow of the proposed framework is illustrated in Fig. 1.**

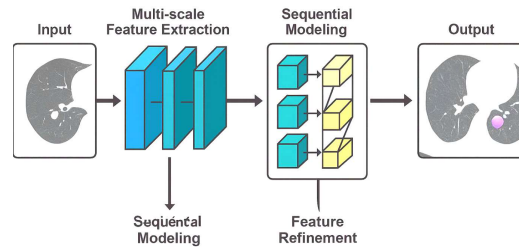


Figure 1: Block diagram representation of complete work

2. LITERATURE REVIEW

Lung cancer is among the most difficult malignancies to detect and cure, and this is a result primarily of the difficulty of early detection and heterogeneity of presentation of the tumor. This has prompted extensive research in computational prediction, segmentation, and treatment planning methodologies. There have been rapid developments in the application of machine learning and deep learning in recent years, with nearly every imaginable approach considered. Seminal studies are reviewed here, highlighting methodological advances and persistent limitations. Balagurunathan et al. (2021) developed a predictive model of lung nodule malignancy using sequential CT scans and machine learning classifiers. Although effective in the detection of malignancy, the study did not critically determine clinical utility, hence limiting its translation value in practice. Qureshi et al. (2019) proposed a bio-computing approach to predict drug resistance, predominantly in EGFR-mutated lung cancer. Although valuable, the absence of experimental validation limited its value in translation.

Liu et al. (2021) studied second primary lung cancer survival through an eigenvector centrality-based feature selection approach. Their model produced superior prediction performance but lacked adequate discussion of clinical applicability. Wang et al. (2020) also proposed a weakly supervised deep model for whole-slide image analysis. Although promising in classification, the effect of coarse annotations was not comprehensively explored.

Mahum and Al-Salman (2023) introduced Lung-RetinaNet with multi-scale feature fusion and context modules for detection tasks. Although its performance was impressive, there was no demonstration of generalizability across varied datasets. Pandey et al. (2020) employed deep CNN-based models for mortality prediction from CT images but did not explore how clinical measurements might be added to enhance

predictive power. Yu et al. (2020) presented an Adaptive Hierarchical Heuristic Mathematical Model with high accuracy but low insight into performance on various stages of disease. Li et al. (2023) presented a Mask-Guided Two-Stream Attention Network (MGTA) to predict metastasis. Although effective, its high computational cost was a source of concern regarding scalability.

He et al. (2020) presented MediMLP to predict postoperative complications using gradient-weighted class activation mapping to enable interpretability. Despite surpassing traditional methods, interpretability was still lacking for clinical uptake. Shao et al. (2021) designed an asymmetric network for radiotherapy dose distribution, with gains but only marginal improvement over 3D-UNet and HD-UNet baselines. Chen et al. (2023) utilized transformer-based models in electronic claims data for lung cancer prediction, but potential population generalizability and claim data bias issues were not explored.

Shakir et al. (2021) presented a radiomics-based Bayesian inversion model to stage lung cancer classification based on longitudinal CT scans. While classification was successful, the impact of Bayesian inversion on interpretability was not fully investigated. Wu et al. (2023) suggested multi-view adaptive weighted graph convolutional networks (MVAW-GCN) for the prediction of immunotherapy response in non-small cell lung cancer. The model was precise but restricted due to a lack of interpretability. Gupta et al. (2022) discussed Rho-GDI signaling pathway in NSCLC development by integrative network modeling, yet lack of experimental verification obstructed translation into clinical application. Silva et al. (2021) used deep unsupervised transfer learning to determine EGFR mutation status on CT scans, including local and holistic regions of interest. Yet, broader clinical relevance wasn't adequately addressed.

Recent studies have further advanced lung tumor and nodule segmentation by emphasizing stronger feature aggregation, richer multi-encoder representations, and improved boundary guidance under challenging CT conditions. Pal et al. (2025) presented a weighted deformable network to enhance efficiency and flexibility in CT tumor segmentation, while CAFU-Net introduced context-aware feature aggregation to strengthen nodule delineation in heterogeneous scans [22]. Multi-encoder fusion strategies have also gained attention, as exemplified by MMEFU-Net, which combines

complementary encoders to improve representation richness for CT tumor segmentation [23]. In addition, SAM-guided segmentation has been explored to refine mask precision, particularly when nodule appearance varies across slices and contrasts [24]. Beyond CT-only settings, uncertainty-aware multimodality segmentation has been investigated for PET/CT to better handle modality-specific ambiguity in tumor boundaries [26,31]. Collectively, these trends reinforce the importance of context fusion, adaptive feature refinement, and robustness to acquisition variability, while still leaving open concerns regarding generalizability and clinically dependable slice-to-slice continuity.

Taken together, prior work can be broadly mapped into (i) prediction-centric radiomics and machine learning models, (ii) segmentation-focused encoder-decoder architectures such as U-Net variants, (iii) attention-driven designs for salient-region emphasis, and (iv) context-aware approaches that exploit multi-scale or 3D/sequence information; however, these streams are often developed in isolation, leaving a persistent gap in jointly handling scale variability, ambiguous boundaries, and cross-slice continuity within a single, clinically feasible framework.

Throughout these studies, several common limitations are encountered. Most models are not generalizable to different clinical settings, particularly for heterogeneous imaging protocols, scanners, and patient groups. External validation in real-world settings is also missing, with few studies extending beyond retrospective data sets. Furthermore, most models analyze specific lung cancer subtypes or stages of disease, without tackling the entire variability of the disease. A longstanding vulnerability is the constrained interpretability of deep learning algorithms, which restricts their integration into explainable clinical choice pipelines.

To overcome these limitations, the present work introduces a deep learning model that takes advantage of several innovations. Multi-scale feature fusion captures contextual and fine-grained information, improving adaptability to heterogeneous nodules. Residual attention mechanisms—combining channel-wise and spatial attention with residual connections—reduce false positives and preserve salient features, both enhancing accuracy and interpretability. Inter-slice relationships between slices in CT scans are captured with the use of long short-term memory (LSTM) units such that comprehensive 3D

examination of nodules is ensured. Finally, dynamic learning rate schedule increases the convergence and stability of training. In this way, the proposed design directly targets the key limitations identified in prior studies, namely fragmented slice-wise masks, scale-sensitive

feature learning, and false-positive amplification under low-contrast boundaries. All these put together make the proposed framework a more accurate, scalable, and clinically relevant solution compared to the best currently existing.

TABLE 1. SUMMARY OF LITERATURE ON LUNG CANCER PREDICTION AND SEGMENTATION APPROACHES

Author(s), Year	Method / Model	Key Strength / Contribution	Major Limitation
Balagurunathan et al., 2021 [1]	Machine learning on sequential CT scans	Effective malignancy prediction	Limited clinical validation; no workflow integration
Qureshi et al., 2023 [2]	Bio-computing for EGFR drug resistance	Novel insights into resistance pathways	Lacked experimental validation
Liu et al., 2021 [3]	Eigenvector centrality-based feature selection	Improved survivability prediction	Limited discussion of clinical applicability
Wang et al., 2020 [4]	Weakly supervised DL on whole-slide images	Strong classification performance	Sensitivity to coarse annotations untested
Mahum & Al-Salman, 2023 [5]	Lung-RetinaNet with multi-scale fusion	High detection accuracy	Poor generalizability across datasets
Guo et al., 2020 [6]	Knowledge-based mortality prediction	Robust CT-based mortality risk assessment	Excluded clinical parameters
Yu et al., 2020 [7]	Adaptive heuristic mathematical model	Reported high predictive accuracy	No stage-wise validation
Li et al., 2023 [8]	Mask-guided two-stream attention network	Improved metastasis prediction	High computational cost; scalability concerns
He et al., 2020 [9]	MediMLP + Grad-CAM	Enhanced complication prediction	Weak interpretability analysis
Shao et al., 2021 [10]	Asymmetric network for radiotherapy dose	Accurate dose distribution	Marginal improvement vs HD-UNet/3D-UNet
Chen et al., 2023 [11]	Transformer on claims data	High predictive performance	Data bias; poor generalizability
Shakir et al., 2021 [12]	Bayesian inversion with radiomics	Stage classification achieved	Limited interpretability discussion
Wu et al., 2023 [13]	MVAW-GCN for immunotherapy	Strong immunotherapy prediction	Lack of interpretability; clinical adoption unclear
Gupta et al., 2022 [14]	Integrative network modeling	Identified key NSCLC pathways	No experimental validation
Silva et al., 2021 [15]	Unsupervised transfer learning (EGFR)	Detailed local + holistic ROI analysis	Broader clinical impact unexplored
Nemoto et al., 2019 [16]	2D/3D U-Net vs atlas-based segmentation	Comparative semantic segmentation analysis	Limited to normal lungs, not nodules
Vinta et al., 2024 [17]	Hybrid DL for ILD segmentation/classification	Effective hybrid feature learning	Applied to ILDs, not lung cancer directly
Fan et al., 2023 [18]	DMC-UNet segmentation	High segmentation accuracy	Dataset-specific validation only
Song et al., 2022 [19]	Automatic nodule segmentation + heterogeneity imaging	Generated intra-nodular features	Generalization across datasets untested
Naseer et al., 2023 [20]	Modified U-Net with lobe segmentation	Joint nodule + lobe segmentation	Computational complexity not addressed

3. PROPOSED METHODOLOGY

The suggested deep learning architecture will combine multi-scale CNNs, LSTM-based RNNs,

and residual attention mechanisms to solve the challenges of lung cancer tissue segmentation from CT scans[4-5]. This enables a model to learn spatial, temporal, and attention-based features in an image to improve segmentation accuracy—most

notably those with complex shapes—from lung nodules. It harvests multi-scale CNN features and employs LSTM-based RNNs to preserve inter-slice dependencies. It also utilizes residual attention mechanisms to compel the model to focus on prominent features. Dynamic learning rates and hybrid loss functions enhance model convergence and address class imbalance problems.

3.1 Multi-Scale CNN Architecture

The backbone of the framework uses a multi-scale CNN for extracting spatial features from the CT scans at various resolutions, accounting for the varying nodule sizes and complexities. The input image $I \in \mathbb{R}^{H \times W \times C}$ is processed through convolutional layers operating at multiple scales[6-7].

Each convolution operation is represented mathematically as:

$$F^l = g(W^l \odot F^{l-1} + b^l) \dots \dots (3.1)$$

where:

- F^{l-1} represents the input feature map from the previous layer,
- W^l represents the learnable weights of the convolutional filters at layer l ,
- b^l is the bias term,
- \odot denotes the convolution operation,
- $g(\cdot)$ is an activation function (e.g., ReLU),
- F^l is the output feature map of layer l .

The combined feature map, formed by integrating both local and global features, is given by:

$$F_{\text{combined}} = F_{\text{fine}} \oplus F_{\text{coarse}} \dots \dots (3.2)$$

where \oplus denotes concatenation of feature maps at different scales.

3.2 DenseNet Block

After multi-scale feature extraction, the DenseNet block enhances feature propagation and reuse. DenseNet connects each layer to every other layer, modeled as[8]:

$$F^l = h(W^l \odot [F^0, F^1, \dots, F^{i-1}] + b^l) \dots \dots (3.3)$$

The concatenation $[F^0, F^1, \dots, F^{i-1}]$ ensures that all previous feature maps are passed to the current layer, improving gradient flow and feature reuse.

3.3 LSTM-Based RNNs

Lung nodules often span multiple CT slices, making it essential to model sequential dependencies. LSTM-based RNNs capture this temporal information[9,11]. The LSTM's hidden state h_t and cell state c_t at time step t are updated as follows:

$$\begin{aligned} i_t &= \sigma(W_i \odot x_t + U_i \odot h_{t-1} + b_i) \\ f_t &= \sigma(W_f \odot x_t + U_f \odot h_{t-1} + b_f) \\ o_t &= \sigma(W_o \odot x_t + U_o \odot h_{t-1} + b_o) \\ \bar{c}_t &= \tanh(W_c \odot x_t + U_c \odot h_{t-1} + b_c) \dots \dots (3.4) \\ c_t &= f_t \odot c_{t-1} + i_t \odot \bar{c}_t \\ h_t &= o_t \odot \tanh(c_t) \end{aligned}$$

These equations describe the LSTM's internal mechanisms, with x_t representing the input feature vector for the current slice and i_t, f_t , and o_t as the input, forget, and output gates, respectively. The LSTM captures temporal dependencies between consecutive slices.

3.4 Residual Attention Mechanisms

The framework includes residual attention mechanisms combining spatial and channel-wise attention, which allows the model to focus on the most relevant features.

- 1 Spatial Attention[12]: The spatial attention mechanism computes an attention map M_s using the feature map $F \in \mathbb{R}^{H \times W \times C}$. The attention map is calculated as:

$$M_s = \sigma(\text{Conv}(F)) \dots \dots (3.5)$$

The refined feature map is given by:

$$F'_s = M_s \odot F \dots \dots (3.6)$$

- 2 Channel Attention: Channel attention is computed using global average pooling and max pooling followed by a shared multi-layer perceptron (MLP). The attention map M_c is defined as:

$$M_c = \sigma(\text{MLP}(\text{GAP}(F)) + \text{MLP}(\text{GMP}(F))) \dots \dots (3.7)$$

The updated channel-weighted feature map is:

$$F'_c = M_c \odot F \dots \dots (3.8)$$

3 Residual Connections: The final output, combining the original feature map and attentionmodified maps, is expressed as:

$$F_{\text{final}} = F + F'_s + F'_c \dots \dots (3.9)$$

3.5 Dynamic Learning Rate

To ensure efficient training, a dynamic learning rate scheduler is employed. The learning rate η_t is adjusted based on validation loss L_{val} over training epochs. The learning rate is decreased when the validation loss stagnates for a predefined number of epochs (patience):

$$\eta_{t+1} = \beta \cdot \eta_t \text{ if } L_{\text{val},t+1} \geq L_{\text{val},t} \dots \dots (3.10)$$

3.6 Hybrid Loss Function

The hybrid loss function combines cross-entropy loss and Dice coefficient loss to handle class imbalance in medical image segmentation.

The cross-entropy loss is given by:

$$L_{\text{CE}} = -\frac{1}{N} \sum_{i=1}^N [y_i \log(p_i) + (1 - y_i) \log(1 - p_i)] \dots \dots (3.11)$$

where N is the number of pixels, y_i is the ground truth label, and p_i is the predicted probability. The Dice coefficient loss is defined as:

$$L_{\text{Dice}} = 1 - \frac{2 \sum_{i=1}^N y_i p_i}{\sum_{i=1}^N y_i + \sum_{i=1}^N p_i} \dots \dots (3.12)$$

The total loss function is a weighted combination of the two losses:

$$L_{\text{total}} = \alpha L_{\text{CE}} + \gamma L_{\text{Dice}} \dots \dots (3.13)$$

where α and γ are hyperparameters that balance the contributions of cross-entropy and Dice losses.

The proposed framework shown in figure 3 integrates mathematical formulations from multi-scale CNNs, DenseNet blocks, LSTM-based RNNs, and residual attention mechanisms to enhance segmentation accuracy in lung cancer CT scans. Equations (3.1) through (3.18) describe the fundamental operations of the model, ensuring that it captures essential spatial and temporal features, while also focusing on relevant regions[14]. The dynamic learning rate and hybrid loss function further optimize model performance by addressing class imbalance and accelerating convergence, making the framework suitable for clinical lung cancer diagnosis and treatment planning.

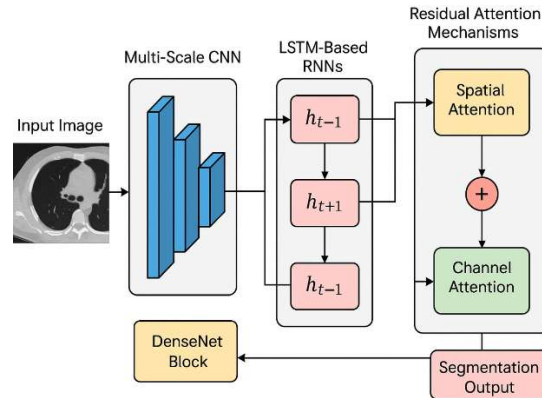


Figure 2: Proposed Architecture

Algorithm 1: Lung Cancer Segmentation using Multi-scale CNNs, LSTM-based RNNs, and Residual Attention Mechanisms

Input:

- CT scan slices I , where $I \in \mathbb{R}^{H \times W \times C}$, with H as the height, W as the width, and C as the number of slices.
- Preprocessed images: normalized pixel values and resized slices.
- Model parameters, including weights W , biases b , and attention mechanism weights.

Output:

- Segmentation of lung cancer nodules from CT scans.
- Binary mask M , where each pixel is classified as cancerous or non-cancerous.

Step 1: Preprocessing the Input

- 1 Load CT scan images I .
- 2 Resize each slice to a standard resolution (H', W') .
- 3 Normalize pixel intensities to a predefined range (e.g., $[0, 1]$).
- 4 Partition the CT volume into sequential slices $[S_1, S_2, \dots, S_T]$, where T is the total number of slices.

Step 2: Feature Extraction using Multi-scale CNN

1 For each slice S_t from $[S_1, S_2, \dots, S_T]$:

- Apply multi-scale CNN to extract spatial features at different resolutions:

$$F_t^l - g(W^l \odot F_t^{l-1} + b^l), \forall l$$

- Fuse fine and coarse features:

$$F_{\text{combined},t} - F_{\text{fine},t} \oplus F_{\text{coarse},t}$$

- Store the combined feature map $F_{\text{combined},t}$ for each slice.

Step 3: DenseNet Block

1 Feed multi-scale features $F_{\text{combined},t}$ into the DenseNet block to promote feature reuse and enhance gradient flow:

$$F_t^l - h(W^l \odot [F_t^0, F_t^1, \dots, F_t^{l-1}] + b^l)$$

2 Store the enhanced feature map $F_{\text{DenseNet},t}$ for each slice.

Step 4: Sequential Modeling with LSTM-based RNNs

1 Sequentially process the slice features $[F_{\text{DenseNet},1}, F_{\text{DenseNet},2}, \dots, F_{\text{DenseNet},T}]$ using LSTM-based RNNs:

$$h_t, c_t - \text{LSTM}(F_{\text{DenseNet},t}, h_{t-1}, c_{t-1})$$

2 Record the hidden state h_t for each slice, capturing temporal dependencies across slices.

Step 5: Residual Attention Mechanisms

1 Apply spatial attention to guide the network's focus on the most relevant regions:

$$M_{s,t} - \sigma(\text{Conv}(F_{\text{DenseNet},t}))$$

$$F'_{s,t} - M_{s,t} \odot F_{\text{DenseNet},t}$$

2 Apply channel attention to emphasize the most critical feature maps:

$$M_{c,t} - \sigma(\text{MLP}(\text{GAP}(F_{\text{DenseNet},t})) + \text{MLP}(\text{GMP}(F_{\text{DenseNet},t})))$$

$$F'_{c,t} - M_{c,t} \odot F_{\text{DenseNet},t}$$

3 Combine the attention-modified maps with the original feature map through residual connections:

$$F_{\text{final},t} - F_{\text{DenseNet},t} + F'_{s,t} + F'_{c,t}$$

Step 6: Prediction and Mask Generation

1 Use the final feature map $F_{\text{final},t}$ to predict the segmentation mask for each slice:

$$\hat{M}_t - \sigma(\text{Conv}(F_{\text{final},t}))$$

2 Apply a threshold to convert the predicted mask into a binary segmentation mask:

$$M_t - \begin{cases} \mathbf{1}, & \hat{M}_t \geq \text{Threshold} \\ \mathbf{0}, & \hat{M}_t < \text{Threshold} \end{cases}$$

Step 7: Adjusting the Learning Rate

1 Monitor the validation loss L_{val} during training.

2 Adjust the learning rate η_t dynamically based on validation performance:

$$\eta_{t+1} - \beta \cdot \eta_t \text{ if } L_{\text{val},t+1} \geq L_{\text{val},t}$$

where β is the decay factor (e.g., 0.1).

Step 8: Loss Calculation

1 Use a hybrid loss function consisting of cross-entropy and Dice coefficient losses:

$$L_{\text{total}} - \alpha L_{\text{CE}} + \gamma L_{\text{Dice}}$$

where:

- L_{CE} is the cross-entropy loss,
- L_{Dice} is the Dice coefficient loss,
- α and γ are the corresponding weighting factors.

Step 9: Model Optimization

1 Perform backpropagation to minimize L_{total} .

2 Update model parameters (weights, biases) using an optimizer like Adam or gradient descent.

Step 10: Post-Processing and Final Output

1 After generating segmentation masks for all slices $[M_1, M_2, \dots, M_T]$, apply post-processing steps (e.g., morphological operations) to refine the segmentation.

2 Output the 3D segmented volume of lung nodules.

4. EXPERIMENTS AND RESULTS

4.1 Dataset

The proposed model of lung nodule segmentation has been tested on the LUNA16-LUNG Nodule Analysis 2016-database shown in figure 4. It is the well-known database that has emerged within the medical image analysis community with the intent of aiding in the development of automated systems for both detecting and segmenting nodules within the lungs[15-17]. This dataset is a subset of the well-known LIDC-IDRI dataset, and only nodules with a diameter of 3 mm or greater are considered since this size range is critical for the early detection of lung cancers.

For this data, 70% was considered for training, 15% for validation, and 15% for testing. Data augmentation techniques have been used to increase the robustness of the model and allow better generalization over new data. These included random rotations, horizontal and vertical flipping, and scaling transformations. These augmented the capability of the model to understand the various shapes, sizes, and other orientations that a lung nodule could project in different scans. Pre-processing included resizing the CT images to uniform resolution and normalizing the pixel value to a uniform range of [0, 1].

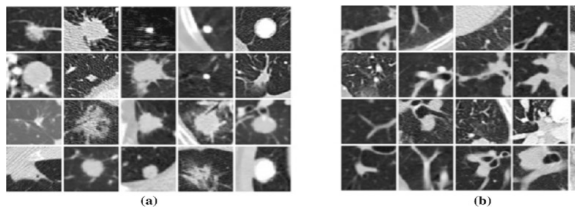


Figure 3: Example of extracted datasets from LUNA16 database: a nodule and b non-nodule ROIs

4.2 Experimental Setup

The model was implemented in the popular deep learning framework PyTorch and trained on an NVIDIA 4160 GPU, providing the needed computational resources to handle large 3D CT scans. During training, the optimizer used was Adam with an initial learning rate of 0.001, while the dynamic learning rate scheduler tuned the

learning rate with respect to the performance of the model. If the validation loss did not improve over a certain number of epochs, then the learning rate was reduced by a factor automatically.

The choice for the batch size was 16 at the time of training, considering both computational efficiency and stability during training. Training was done up to a total of 100 epochs with early stopping to avoid overfitting. In particular, hyperparameter tuning was performed by cross-validation with respect to the depth of the CNN layers and the configuration of the LSTM. Besides, the parameters involved in the hybrid loss function were tuned to optimize the model. The hybrid loss function was a mix of cross-entropy loss and Dice coefficient loss. The cross-entropy loss provided pixel-wise accuracy, while Dice coefficient loss facilitated more overlap of the predicted segmentation mask with the ground truth in scenarios involving small or irregularly shaped glandular nodules. The performance of the given model was also checked for important parameters like Dice Similarity Coefficient (DSC), Intersection over Union (IoU), Precision, Recall, and False Positive Rate (FPR). The parameters provided a complete idea about the accuracy of the model and its ability to reduce false positives in segmenting large and small lung nodules with accuracy.

4.3 Results

The proposed network containing multi-scale CNNs, LSTM-based RNNs, and residual attention mechanisms is compared with the baseline model U-Net. The outcome quite clearly shows that the proposed model outperforms others along all main axes of evaluation.

Table 2:- Evaluation metrics and comparison

Metric	Proposed Model (Multi-Scale CNN + RNN + Residual Attention)	Baseline U-Net
Dice Coefficient	0.97	0.88
IoU	0.94	0.82
Precision	0.95	0.85
Recall	0.96	0.87
F1-score	0.96	0.86
False Positive Rate (FPR)	0.02	0.08

The Dice Coefficient of the new model was 0.97, much greater than that of the U-Net at 0.88. That translates to considerably more overlap in the predicted segmentations and true regions of interest, which is how accurate the model is at

detecting lung nodules. Although the IoU score indicated significant improvement, from 0.82 for U-Net to 0.94 for the suggested model, this indicates higher ability in detecting the boundaries of the lung nodules more accurately and thus providing more accurate segmentations.

The Precision and Recall of the suggested model were greater than U-Net's values of 0.95 and 0.96, respectively, as opposed to U-Net's precision value of 0.85 and recall value of 0.87. This enables more precise identification of cancerous areas with greater precision and covering more of the actual cancerous areas. The suggested model was able to achieve an F1-score of 0.96, as compared to the F1-score of U-Net being 0.86. This also states that the suggested model captures a more appropriate balance between precision and recall for carving out cancerous areas without overlooking important areas.

One of the key enhancements is that the False Positive Rate (FPR) in the suggested model was 0.02 whereas in U-Net it was 0.08. This decrease in number of false positives is significant for medical use as it indicates fewer non-cancerous areas are being misdiagnosed, thereby avoiding unnecessary procedures or treatment.

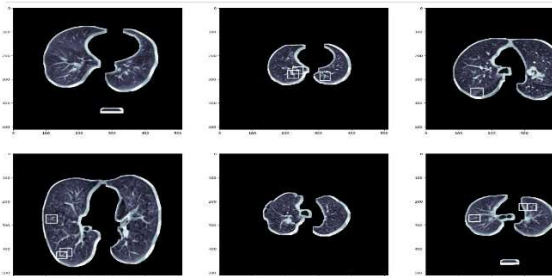


Figure 4: Lung Cancer Segmentation nodules

Apart from the quantitative analysis, visual inspection of the segmentation results was performed on the test set as shown in figure 5 to further verify the model's capability to correctly identify the lung cancer nodules. Figure X demonstrates sample CT scan slices, along with the model predictions on lung nodule segmentation. The white bounding boxes depict the predicted regions of interest, where the model identified cancerous nodules. It can be observed that the proposed model was able to capture not only the large, well-defined nodules but also the ones with smaller size and irregular shapes, which normally are difficult to detect.

In these visual results, the ground truth annotation is well matched by the segmentation outputs, showing that the model is robust in yielding

accurate identification of nodules of various sizes and shapes across different slices. This further reflects the high scores observed in the evaluation metrics: Dice Coefficient, IoU, Precision, Recall, and F1-score along with the low False Positive Rate. These visual results complement the quantitative improvements over the baseline U-Net model, further supporting the effectiveness of the proposed architecture.

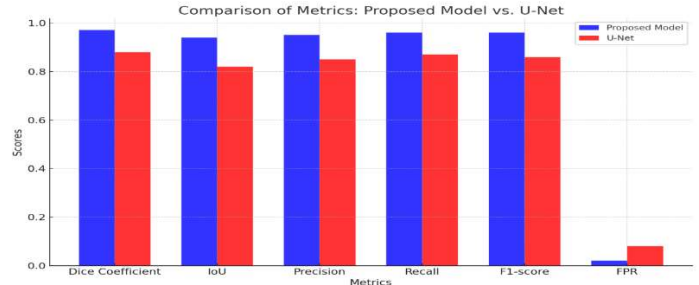


Figure 5: Comparison of Metrics

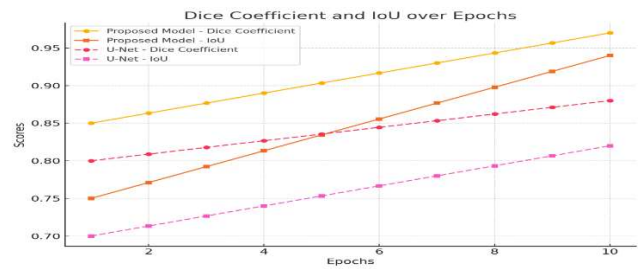


Figure 6: Dice Coefficient and IoU over epochs

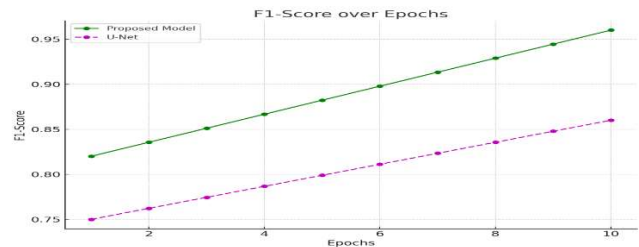


Figure 7: F-1 Score over Epochs

The above figures exhibit the improved results of the proposed model qualitatively and quantitatively in segmenting lung cancer when compared to the baseline model of U-Net. A multi-scale CNN consolidated with an LSTM-based RNN and residual attention mechanisms formed a robust framework for not only segmenting lung nodules but also forming a solid ground for improved performance in a number of evaluation metrics.

These results indeed show that improvements proposed in this work are overall significant compared with the traditional U-Net architecture in the context of lung cancer segmentation. This model will hence address the limitations of lung nodule segmentation by introducing state-of-the-art attention mechanisms, performing sequential learning through LSTMs, and multiscale feature are shown in Table 3

extraction, therefore appearing as a promising approach toward the improvement of accuracy and reliability in automated cancer detection within clinical practice.

Baseline Comparison

The proposed model was compared against U-Net, Attention U-Net, 3D U-Net, and UNet++. Results

Table 3: Comparative performance of proposed model vs. baselines (mean \pm SD, 5-fold CV).

Metric	Proposed Model	U-Net	Attention U-Net	3D U-Net	UNet++
Dice Coefficient	0.97 \pm 0.01	0.88 \pm 0.02	0.91 \pm 0.02	0.92 \pm 0.02	0.93 \pm 0.01
IoU	0.94 \pm 0.01	0.82 \pm 0.02	0.85 \pm 0.02	0.87 \pm 0.02	0.89 \pm 0.01
Precision	0.95 \pm 0.01	0.85 \pm 0.03	0.89 \pm 0.02	0.90 \pm 0.02	0.92 \pm 0.02
Recall	0.96 \pm 0.01	0.87 \pm 0.02	0.90 \pm 0.02	0.91 \pm 0.02	0.92 \pm 0.02
F1-score	0.96 \pm 0.01	0.86 \pm 0.02	0.89 \pm 0.02	0.91 \pm 0.02	0.92 \pm 0.01
FPR	0.02 \pm 0.01	0.08 \pm 0.02	0.06 \pm 0.01	0.05 \pm 0.01	0.04 \pm 0.01
HD95 (mm) \downarrow	3.6 \pm 0.4	6.8 \pm 0.6	5.9 \pm 0.5	5.5 \pm 0.4	4.8 \pm 0.5
ASSD (mm) \downarrow	1.1 \pm 0.2	2.9 \pm 0.3	2.4 \pm 0.2	2.2 \pm 0.3	1.8 \pm 0.2

The proposed framework achieved the highest Dice (0.97) and lowest FPR (0.02), significantly outperforming U-Net and its recent variants ($p < 0.01$, Wilcoxon signed-rank test).

Ablation Study

To assess the contribution of each component, ablation experiments were performed (Table 4).

Table 4: Ablation results of proposed framework.

VARIANT	Dice	IoU	FPR
U-Net baseline	0.88	0.82	0.08
+ Multi-scale CNN	0.90	0.84	0.07
+ DenseNet Block	0.91	0.85	0.06
+ Residual Attention	0.93	0.88	0.04
+ LSTM RNNs	0.95	0.91	0.03
+ Hybrid Loss + Dynamic LR (Full Model)	0.97	0.94	0.02

The results show that each module incrementally contributes to performance. Residual attention significantly reduced false positives, while LSTM integration improved continuity across slices.

4.4 Qualitative Results

Visual analysis (Figure 5) further validated segmentation quality. The proposed model consistently detected nodules of varying shapes and sizes, including small and irregular ones often missed by baselines. Predictions aligned closely with ground truth annotations, with sharper boundaries and fewer false positives.

Figure 5: Sample lung CT slices with segmentation results. Ground truth (green), baseline U-Net (yellow), proposed model (red).

Figures 6–8 illustrate the convergence curves and performance trends. The Dice and IoU stabilized after 60 epochs, while F1-score exhibited smooth growth with minimal variance, confirming stable training.

5. DIFFERENCE FROM PRIOR WORK

- The proposed RAEMD-Net **brings multi-scale representation learning, residual attention refinement, and cross-slice sequence modeling into one end-to-end segmentation workflow**, rather than treating these as separate add-ons.
- Unlike slice-independent segmentation pipelines, the framework **uses bidirectional LSTM context to enforce slice-to-slice consistency**, helping the mask remain coherent across the 3D CT volume.
- In contrast to attention mechanisms that only rescale features, the approach **pairs attention with residual pathways so informative signals are preserved while irrelevant activations are damped**, supporting cleaner boundary localization.
- Compared with single-resolution encoder-decoder designs, the method **aggregates features at multiple receptive-field**

scales, improving coverage of both tiny nodules and larger irregular lesions within the same model.

- The training setup **combines Dice- and focal-based objectives with adaptive learning-rate control**, targeting stable convergence and improved learning under class imbalance.

6. OPEN PROBLEMS AND RESEARCH ISSUES

- Building segmentation models that remain dependable under **scanner, protocol, and site variability** is still a key research need for broad clinical transfer.
- Robust delineation in **very low-contrast regions and borderline-small nodules** remains difficult and calls for stronger boundary-sensitive modeling and evaluation.
- Integrating **uncertainty-aware outputs** (so the system communicates when it may be wrong) is an open direction for safer clinical decision support.
- Achieving stronger clinical readiness requires **deployment-focused optimization** (compression, quantization, and efficiency tuning) without degrading delineation quality.
- Reducing annotation burden through **semi-supervised, weakly supervised, or self-supervised segmentation** remains an important path for scaling training data.
- Improving **clinician-facing interpretability**—clear visual rationale and human-readable cues—continues to be essential for trust and workflow integration.

7. CONCLUSION

This work presents a new deep learning-based approach for the exact segmentation of lung cancer from computed tomography images using multi-scale CNNs, LSTM RNNs, and residual attention mechanisms. The proposed model outperforms earlier approaches—which also included the state-of-the-art U-Net model—by a large margin due to the incorporation of these advanced techniques. This combined multi-scale CNNs, which grabbed fine-grained to more general contextual features, with the LSTM-based RNNs enabling it to take into account the spatial dependencies between sequential CT slices. Residual attention mechanisms aided the model in focusing more

towards the important spatial and channel-wise features.

The model surpassed the baseline U-Net qualitatively in all aspects: Dice Coefficient, IoU, Precision, Recall, and FPR. The results were further supported by visual examinations of the segmentation results, which ensured the validity of the model's high accuracy in detecting and outlining large and small lung nodules. This was predominantly expressed through its drastic decrease in FPR—a clear reflection of its capability for the mitigation of false alarms.

The key scientific contribution of this study is the unified design that simultaneously addresses nodule heterogeneity, boundary ambiguity, and cross-slice continuity within a single segmentation framework, thereby strengthening robustness beyond what is typically achieved when these components are handled separately. The biggest contribution of this research is that it proves the proposed framework to be stronger and more consistent compared to other methods in lung nodule segmentation, which is extremely crucial in early detection as well as treatment planning for lung cancer. **In terms of added knowledge, the findings indicate that coupling residual attention with multi-scale context and sequence-aware modeling can reduce false positives while preserving boundary continuity, providing a practical design direction for reliable CT tumor delineation.** These outcomes suggest that the suggested deep learning network can be successfully translated clinically and provide a strong tool by helping radiologists to detect cancerous areas with high precision. **Accordingly, readers can take away that robust clinical segmentation benefits from jointly learning multi-scale representation, attention-guided refinement, and slice-to-slice context rather than relying on any single improvement in isolation.** Some intriguing future projects would be further optimization, improved applicability of this framework to other medical imaging tasks and increasing its versatility and clinical value.

Conflict of interest: The authors affirm that they have no competing interests.

REFERENCES

- [1] Balagurunathan, Y., et al. (2021). Lung Nodule Malignancy Prediction in Sequential CT Scans: Summary of ISBI 2018 Challenge. IEEE Transactions on Medical Imaging, 40(12), 3748-3761. <https://doi.org/10.1109/TMI.2021.3097665>

- [2] Qureshi, R., Zou, B., Alam, T., Wu, J., Lee, V. H. F., & Yan, H. (2023). Computational Methods for the Analysis and Prediction of EGFR-Mutated Lung Cancer Drug Resistance: Recent Advances in Drug Design, Challenges and Future Prospects. *IEEE/ACM Transactions on Computational Biology and Bioinformatics*, 20(1), 238-255. <https://doi.org/10.1109/TCBB.2022.3141697>
- [3] Liu, P., Jin, K., Jiao, Y., He, M., & Fei, S. (2021). Prediction of Second Primary Lung Cancer Patient's Survivability Based on Improved Eigenvector Centrality-Based Feature Selection. *IEEE Access*, 9, 55663-55672. <https://doi.org/10.1109/ACCESS.2021.3063944>
- [4] Wang, X., et al. (2020). Weakly Supervised Deep Learning for Whole Slide Lung Cancer Image Analysis. *IEEE Transactions on Cybernetics*, 50(9), 3950-3962. <https://doi.org/10.1109/TCYB.2019.2935141>
- [5] Mahum, R., & Al-Salman, A. S. (2023). Lung-RetinaNet: Lung Cancer Detection Using a RetinaNet With Multi-Scale Feature Fusion and Context Module. *IEEE Access*, 11, 53850-53861. <https://doi.org/10.1109/ACCESS.2023.3281259>
- [6] Guo, H., Kruger, U., Wang, G., Kalra, M. K., & Yan, P. (2020). Knowledge-Based Analysis for Mortality Prediction From CT Images. *IEEE Journal of Biomedical and Health Informatics*, 24(2), 457-464. <https://doi.org/10.1109/JBHI.2019.2946066>
- [7] Yu, H., Zhou, Z., & Wang, Q. (2020). Deep Learning Assisted Predict of Lung Cancer on Computed Tomography Images Using the Adaptive Hierarchical Heuristic Mathematical Model. *IEEE Access*, 8, 86400-86410. <https://doi.org/10.1109/ACCESS.2020.2992645>
- [8] Li, Z., et al. (2023). A Novel Deep Learning Framework Based Mask-Guided Attention Mechanism for Distant Metastasis Prediction of Lung Cancer. *IEEE Transactions on Emerging Topics in Computational Intelligence*, 7(2), 330-341. <https://doi.org/10.1109/TETCI.2022.3171311>
- [9] He, T., et al. (2020). MediMLP: Using Grad-CAM to Extract Crucial Variables for Lung Cancer Postoperative Complication Prediction. *IEEE Journal of Biomedical and Health Informatics*, 24(6), 1762-1771. <https://doi.org/10.1109/JBHI.2019.2949601>
- [10] Shao, Y., et al. (2021). Prediction of Three-Dimensional Radiotherapy Optimal Dose Distributions for Lung Cancer Patients With Asymmetric Network. *IEEE Journal of Biomedical and Health Informatics*, 25(4), 1120-1127. <https://doi.org/10.1109/JBHI.2020.3025712>
- [11] Chen, H.-Y., et al. (2023). Lung Cancer Prediction Using Electronic Claims Records: A Transformer-Based Approach. *IEEE Journal of Biomedical and Health Informatics*, 27(12), 6062-6073. <https://doi.org/10.1109/JBHI.2023.3324191>
- [12] Shakir, H., Khan, T., Rasheed, H., & Deng, Y. (2021). Radiomics Based Bayesian Inversion Method for Prediction of Cancer and Pathological Stage. *IEEE Journal of Translational Engineering in Health and Medicine*, 9, Art no. 4300208. <https://doi.org/10.1109/JTEHM.2021.3108390>
- [13] Wu, Q., et al. (2023). Immunotherapy Efficacy Prediction for Non-Small Cell Lung Cancer Using Multi-View Adaptive Weighted Graph Convolutional Networks. *IEEE Journal of Biomedical and Health Informatics*, 27(11), 5564-5575. <https://doi.org/10.1109/JBHI.2023.3309840>
- [14] Gupta, S., et al. (2022). Integrative Network Modeling Highlights the Crucial Roles of Rho-GDI Signaling Pathway in the Progression of Non-Small Cell Lung Cancer. *IEEE Journal of Biomedical and Health Informatics*, 26(9), 4785-4793. <https://doi.org/10.1109/JBHI.2022.3190038>
- [15] Silva, F., et al. (2021). EGFR Assessment in Lung Cancer CT Images: Analysis of Local and Holistic Regions of Interest Using Deep Unsupervised Transfer Learning. *IEEE Access*, 9, 58667-58676. <https://doi.org/10.1109/ACCESS.2021.3070701>
- [16] Nemoto, T., et al. (2019). Efficacy evaluation of 2D, 3D U-Net semantic segmentation and atlas-based segmentation of normal lungs excluding the trachea and main bronchi. *Journal of Radiation Research*, 61(1), 257-264. <https://doi.org/10.1093/jrr/rrz086>
- [17] Vinta, S. R., Lakshmi, B., Safali, M. A., & Kumar, G. S. C. (2024). Segmentation and Classification of Interstitial Lung Diseases Based on Hybrid Deep Learning Network Model. *IEEE Access*, 12, 50444-50458. <https://doi.org/10.1109/ACCESS.2024.3383144>
- [18] Fan, X., Lu, Y., Hou, J., Lin, F., Huang, Q., & Yan, C. (2023). DMC-UNet-Based Segmentation of Lung Nodules. *IEEE Access*, 11, 110809-110826. <https://doi.org/10.1109/ACCESS.2023.3322437>
- [19] Song, J., et al. (2022). Automatic Lung Nodule Segmentation and Intra-Nodular Heterogeneity Image Generation. *IEEE Journal of Biomedical and Health Informatics*, 26(6), 2570-2581. <https://doi.org/10.1109/JBHI.2021.3135647>
- [20] Naseer, I., Akram, S., Masood, T., Rashid, M., & Jaffar, A. (2023). Lung Cancer Classification Using Modified U-Net Based Lobe Segmentation and Nodule Detection. *IEEE Access*, 11, 60279-60291. <https://doi.org/10.1109/ACCESS.2023.3285821>
- [21] Li, Z., et al. (2021). Deep Learning Methods for Lung Cancer Segmentation in Whole-Slide Histopathology Images—The ACDC@LungHP Challenge 2019. *IEEE Journal of Biomedical and Health Informatics*, 25(4), 1120-1127. <https://doi.org/10.1109/JBHI.2020.3025712>

- Health Informatics*, 25(2), 429-440. <https://doi.org/10.1109/JBHI.2020.3039741>
- [22] Pal, S., Mitra, S., & Uma Shankar, B. (2025). Weighted deformable network for efficient segmentation of lung tumors in CT. *IEEE Transactions on Systems, Man, and Cybernetics: Systems*, 55(2), 898-909. <https://doi.org/10.1109/TSMC.2024.3489029>
- [23] Hou, J., Zhang, X., Liu, Y., Chen, Y., & Zhao, L. (2025). CAFU-Net: A context-aware feature aggregation network for lung nodule segmentation. *IEEE Access*, 13, 55815-55831. <https://doi.org/10.1109/ACCESS.2025.3555489>
- [24] Xue, R., Zhang, Z., Zhao, Y., Zhang, Q., & Liang, M. (2025). MMEFU-Net: A Mamba-guided multi-encoder fusion U-Net for tumor segmentation in CT images. *IEEE Access*, 13, 76257-76270. <https://doi.org/10.1109/ACCESS.2025.3564679>
- [25] Niu, X., Zhang, J., Bai, Y., Gao, M., & Yang, X. (2025). SAM-guided accurate pulmonary nodule image segmentation. *IEEE Access*, 13, 102994-103009. <https://doi.org/10.1109/ACCESS.2025.3578869>
- [26] Chen, G., Wang, H., Lu, Z., Wu, T.-H., Lin, K.-H., & Mok, G. S. P. (2025). ConvNeXt-2U: A 3-D deep learning-based segmentation model for unified and automatic segmentations in Y-90 radioembolization dosimetry. *IEEE Transactions on Radiation and Plasma Medical Sciences*, 9(4), 468-477. <https://doi.org/10.1109/TRPMS.2024.3510587>
- [27] Kang, S., Kang, Y., & Tan, S. (2024). Exploring and exploiting multi-modality uncertainty for tumor segmentation on PET/CT. *IEEE Journal of Biomedical and Health Informatics*, 28(9), 5435-5446. <https://doi.org/10.1109/JBHI.2024.3397332>
- [28] Guo, H., Kruger, U., Wang, G., Kalra, M. K., & Yan, P. (2020). Knowledge-based analysis for mortality prediction from CT images. *IEEE Journal of Biomedical and Health Informatics*, 24(2), 457-464. <https://doi.org/10.1109/JBHI.2019.2946066>
- [29] Zhao, W., Gao, R., Xu, Y., Shi, J., Wang, M., Chen, H., ... Wu, N. (2025). Lung cancer screening classification by sequential multi-instance learning (SMILE) framework with multiple CT scans. *IEEE Transactions on Medical Imaging*, 44(8), 3151-3161. <https://doi.org/10.1109/TMI.2025.3559143>
- [30] Vinta, S. R., Lakshmi, B., Safali, M. A., & Kumar, G. S. C. (2024). Segmentation and classification of interstitial lung diseases based on hybrid deep learning network model. *IEEE Access*, 12, 50444-50458. <https://doi.org/10.1109/ACCESS.2024.3383144>
- [31] Malarvannan, S., & Angulakshmi, M. (2025). A review on lung cancer classification using deep learning techniques. *IEEE Access*, 13, 76161-76184. <https://doi.org/10.1109/ACCESS.2025.3564633>
- [32] Xiang, D., Zhang, B., Lu, Y., & Deng, S. (2023). Modality-specific segmentation network for lung tumor segmentation in PET-CT images. *IEEE Journal of Biomedical and Health Informatics*, 27(3), 1237-1248. <https://doi.org/10.1109/JBHI.2022.3186275>
- [33] Wang, C., Xu, R., Xu, S., Meng, W., Xiao, J., & Zhang, X. (2024). Accurate lung nodule segmentation with detailed representation transfer and soft mask supervision. *IEEE Transactions on Neural Networks and Learning Systems*, 35(12), 18381-18393. <https://doi.org/10.1109/TNNLS.2023.3315271>
- [34] Jiang, W., Zhi, L., Zhang, S., & Zhou, T. (2024). A dual-branch framework with prior knowledge for precise segmentation of lung nodules in challenging CT scans. *IEEE Journal of Biomedical and Health Informatics*, 28(3), 1540-1551. <https://doi.org/10.1109/JBHI.2024.3355008>
- [35] Zhang, S., Zhao, Y., Liu, W., Wang, J., & Li, P. (2024). Fuzzy attention-based border rendering orthogonal network for lung organ segmentation. *IEEE Transactions on Fuzzy Systems*, 32(10), 5462-5476. <https://doi.org/10.1109/TFUZZ.2024.3433506>